An Experimental and Numerical Study on the Lateral Stiffness Limits of Straddle-type Monorail Tour-transit Systems

Hong Zhang , Pengjiao Wang , Qin Li , Junhui Jin , Shiqi Wei , Fengqi Guo * , Cheng Feng , Qun Deng

Posted Date: 5 September 2024

doi: 10.20944/preprints202409.0428.v1

Keywords: monorail tour-transit system; lateral stiffness; co-simulation; dynamic response; sensitivity analysis

Article

An Experimental and Numerical Study on the Lateral Stiffness Limits of Straddle-Type Monorail Tour-Transit Systems

Hong Zhang [1], Pengjiao Wang [2], Qin Li [3], Junhui Jin [4], Shiqi Wei [2], Fengqi Guo [2,*], Cheng Feng [3] and Qun Deng [3]

[1] College of Mechanical and Intelligent Manufacturing, Central South University of Forestry and Technology, Changsha 410075, China
[2] School of Civil Engineering, Central South University, Changsha, 410075, China
[3] 3rd Construction Co. Ltd. of China Construction 5th Engineering Bureau, Changsha 410004, China
[4] Zhuzhou CRRC Special Equipment Technology Co., Ltd., Zhuzhou 412001, China
* Correspondence: fengqiguo@csu.edu.cn

Abstract: The development of straddle-type monorail tour-transit systems (MTTSs) has received keen attention, raising the need for revisions on related design codes. This work presents a comprehensive assessment of the lateral stiffness limit of steel substructures in MTTSs. Firstly, a wind–vehicle–bridge coupling model was established, integrating multibody dynamics and finite element methods. This model was then validated against field test results, considering measured track irregularities as the excitation. Afterwards, a trend analysis and a variance-based sensitivity analysis was performed to investigate the effect of various factors on the dynamic response of MTTS. Referring to existing specifications, an evaluation index for the lateral stiffness of pier columns and track beams was proposed. Results indicate that the pier height significantly impacts the lateral displacement of the pier top, accounting for 87% of the first-order sensitivity index and 75% of the total sensitivity index. In comparison, the lateral stiffness of track beams contributes over 70% to the maximum lateral acceleration and displacement at the mid-span. Finally, the lateral limited values for the displacement at the pier top and the deflection–span ratio of the track beam were determined as 8.04 mm and L/4200, respectively. These findings can serve as valuable references for future research and designs in this field.

Keywords: monorail tour-transit system; lateral stiffness; co-simulation; dynamic response; sensitivity analysis

1. Introduction

The straddle-type monorail tour-transit system (MTTS) has developed rapidly in recent years. At present, there are more than 30 MTTS projects under construction or operation over the world [1]. It uses lightweight steel box girders as the supporting track beam and steel column as the substructures, which is easy for construction, has good ornamental characteristics, and is very suitable for scenic areas. With these configurations, the weight of the track beam of MTTS is light, and the overall stiffness is relatively low. Compared with the supporting structures of general transportation systems, the dynamic response of the track beam of MTTS is more significant. In particular, the lateral stiffness is an essential factor affecting the smoothness and comfort of train operation and hence, the related limited values must be reasonably determined. However, the design code for MTTS, i.e., the "Large-scale amusement device safety code (GB 8408-2018) [2]", does not have specific regulations in this respect. Of course, provisions in relevant codes (e.g., design code for urban rail transit bridge (GB/T 51234-2017) [3] and monorail in urban transit systems (GB 50458-2022) [4]) can be used for reference. However, practical use has proven that these codes are not completely applicable because of the structural diversity in various transit systems and the design concepts of

 doi:10.20944/preprints202409.0428.v1

different codes. Therefore, it is important to carry out targeted research and improve relevant design standards to promote the development of modern tourism systems.

In general, existing studies on the dynamic responses of transportation systems were conducted through numerical simulations, e.g., using finite element method (FEM) and multi-body dynamics (MBD). For example, Gao et al. developed a co-simulation model using ANSYS (FEM software) and SIMPACK (MBD software) to study the effects of vehicle speed and bridge pier height on a rail system [5]. Liu studied the dynamic response of a T-girder continuous rigid frame bridge: by using a computational fluid dynamics (CFD) software, the aerodynamic parameters and their effects of the bridge under passing vehicles were simulated [6]. Furthermore, many studies have been able to consider the coupling effect of various loadings. For example, Miao et al. [7] established a refined space vibration model of a wind-vehicle-bridge system with time-varying characteristics to investigate the dynamic features of bridges. Huang et al. [8] utilized a co-simulation method to analyse the mechanical properties of bridges under wind–vehicle–bridge coupling actions. Chen et al. [9] and Wang et al. [10] studied the aerodynamic performance of a vehicle–bridge system under the action of a crosswind. Zou et al. [11] developed a joint model to analyse the dynamic response of a wind—monorail car—suspended bridge system under wind loadings. In addition, laboratory tests on the coupling system were reported. Luo et al. [12] measured the aerodynamic coefficients of relevant bridge and vehicle models under the action of crosswind through a wind tunnel test. Jiang et al. [13] focused on the most unfavourable load that long-span bridges bore when vehicles and subways were in operation at the same time, and relevant models were established for dynamic response studies. Guo et al. [14] performed wind tunnel tests and numerical simulations to investigate the dynamic characteristics of bridge; the wind–car–bridge coupling model was also developed via FEM and CFD. It should be noted that these studies are dominantly focus on rail transportations, results in general monorail system are still limited, not to mention relevant studies on MTTS. Nevertheless, the methodologies of general transportation system can be used as great reference.

In terms of lateral stiffness limit, a perspective more inclined towards practical application, research has made great progress on general transit systems. In general, the main body of vehicle can be simulated or constructed by using MBD. Then, a targeted dynamic evaluation system can be proposed based on the results of the dynamic response of vehicle and bridges [15]. Xiang et al. [16] investigated the lateral stiffness limit of a suspension bridge through a combination of wind tunnel test and numerical simulation. Zhou et al. [17] investigated the effects of the height of the bridge pier and the lateral stiffness of the bridge beam on the dynamic response of a vehicle-bridge system. Zhu et al. [18] developed multiple suspension bridge models and investigate various methods to improve the structural stiffness of the railway bridges. Liu et al. [19] proposed an analytical model to quantitatively analyse the influence and mechanism of several important parameters on the mapped deformation of the rail, including the lateral beam deformation and the lateral stiffness of fasteners. Wang et al. [20] performed numerical simulations of the coupled vibration of 12 track-beam systems with different stiffnesses. In the study, track irregularities and wind-induced lateral loads were considered. Yan et al. [21] investigated the design value of the torsional stiffness reduction factor for the serviceability limit states. CARDEN et al. [22] proposed a simplified calculation method based on the elastic stress and stiffness of bridge beams, and the results were found comparable with those obtained by FEM.

To sum up, existing studies on the dynamic response of monorail systems, including MTTS, and effects of lateral stiffness of monorail bridge, i.e., track beams and piers, are limited. Research have reported field tests and numerical simulations of the monorail systems considering track irregularities [23-26], wind loadings [27], and ground motions [28]. Moreover, the usage of FEM and MBD on monorails have been verified, providing an effective method for investigating the dynamic effects of MTTS. To the best of our knowledge, no existing studies have focused on the determination of lateral limited values of MTTS.

On the basis of a comprehensive analysis of the existing research and considering the unique structural configurations of MTTS, this work employs FEM and MBD software to establish a wind–

 doi:10.20944/preprints202409.0428.v1

vehicle–bridge coupling model of MTTS. The effects of variables such as vehicle load and track beam lateral stiffness on vehicle running stability, acceleration, and the lateral force of guide wheels and stabilizing wheels are investigated. Through numerical simulation and parametric analysis, the lateral deflection–span ratio limit and the lateral displacement limit of the pier top were determined based on the riding comfort standard, i.e., the mid-span acceleration of the monorail track beam and the lateral force limit of the monorail train wheels. The results of the study can improve the problem of unclear limits of lateral stiffness of MTTS, which can provide a reference for related research and design.

2. Methodologies

2.1 Wind-Vehicle-Bridge Coupling Mode

2.1.1 Modelling Track Beams

For easy demonstration, a one-connection five-span curve bridge in the Dajueshan project in Jiangxi, China is taken as the example. The curve radius of track beam is 30 m, the span of a single girder is 10 m, and the bridge pier is a single column with a pier height of 2 m. A solid element with 6 degrees of freedom in ABAQUS (FEM software) was chosen to model the monorail substructures (track beams and piers). The cross-section of track beams, pier–column elevation and FE model of the track beam structure are shown in Figure 1.

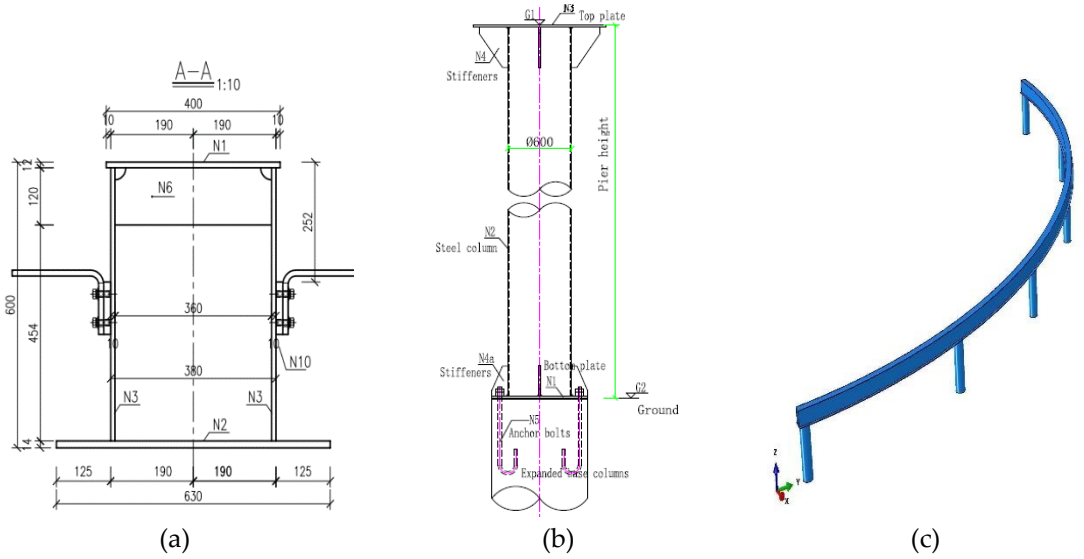

Figure 1. Representative design diagrams and numerical model of monorail substructures. (a) Cross-section of the track beam; (b) design diagram of the pier; (c) finite element model.

2.1.2 Modelling Monorail Trains

Owing to the complexity of the vehicle system, necessary simplifications should be performed to efficiently simulate their mechanical characteristics, e.g., using MBD. In this work, the mass, geometric characteristics, and dynamic characteristics of each component of the monorail train were considered. According to the principle of MBD, main bodies, such as the car body and bogies, are modelled as rigid components, which are then connected by springs and dampers. The main components of a bogie are the frame, bolster, spring and other shock damping equipment; the power drive device; and three types of wheels: travelling wheels, steering wheels, and stabilizing wheels. To improve the accuracy of the model, springs and other shock damping equipment are simulated via the force element in SIMPACK.

The modelling of the monorail train adopts the substructure technic in SIMPACK. Specifically, a bogie is firstly constructed and transferred as a substructure; then, two identical substructures

Preprints.org (www.preprints.org) | NOT PEER-REVIEWED | Posted: 5 September 2024 doi:10.20944/preprints202409.0428.v1

(bogie) can be used to model one carriage, along with the car body. Similarly, the carriage can be transformed into a substructure and be used to model the entire train. The main modelling parameters were provided by the Zhuzhou CRRC Special Equipment Technology Co., Ltd. The developed MBD models of a 4-carriage monorail system are shown in Figure 2.

(a) (b)

Figure 2. Onsite monorail train and its MBD model (a) A train in the Dajueshan project; (b) MBD model.

2.1.3 Coupling Model

During the actual operation of an MTTS, the track beam will be disturbed by the pulsation wind component in the crosswind, which will generate lateral rocking motion, thereby reducing ride comfort and running stability. In this work, the Kamal spectrum considering the height factor was chosen as the fluctuating wind spectrum for loading, and the harmonic synthesis method was used for wind field simulation. The wind force experienced by an MTTS in a natural wind field can usually be decomposed into three parts: aerodynamic drag (FD), aerodynamic lift (FL) and the aerodynamic moment (FM). The values of the three-component force coefficients are collected from numerical simulations via the FLUENT software, and the details are shown in Table 1 below.

Table 1. Aerodynamic coefficients of vehicles and bridges.

Type	FD	FL	FM
Vehicle	1.53	0.68	-0.03
Bridge	1.12	-0.15	-0.04

Previous studies have reported the results from field measurement, including the track irregularities and dynamic responses of MTTS, and the spectrum of longitudinal and horizontal level irregularity were estimated [24-25]. On the basis of measured results in several projects, an evaluation system for the spectrum of track irregularity has been proposed. The system contains spectra of six levels to meet various actual conditions of the track lines in practical projects, see Figure 3. To reflect the general state of track irregularity in actual operation projects, the most widely used and representative C-level spectrum is chosen in the present study for subsequent coupling analysis.

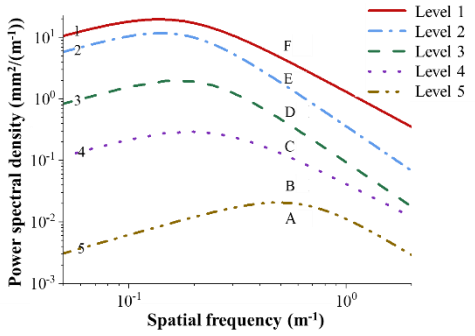

 doi:10.20944/preprints202409.0428.v1

Figure 3. Integrating different level track irregularities.

In the track beam model, the wheel–rail forces are transferred, and the interaction between the vehicle and the track is simulated via substructure analysis, fixed master nodes, an interpolation algorithm, elastic deformation, and dynamic interaction. Similar modelling methods have been validated in existing studies [25-28]. The simulation results of the Kamal spectrum are obtained via the harmonic synthesis method, and the wind load time history is directly applied to the car body and track beam via force elements. After defining the spectral formula, the track irregularity can be retrieved in the form of excitation type in SIMPACK.

2.2 Model Validation

2.2.1 Test Site Information

To validate the effectiveness of the developed coupling model, an on-site dynamic response test was conducted in the MTTS test-line located in Zhuzhou City, China. The construction standard of the test line is the same as that of the actual MTTS project. In other words, the configuration of the trains and track girders is consistent with the actual project. During the test of track beams, the focus was placed on the vertical displacement and lateral and vertical acceleration of the mid-span cross section. The location of measuring points was determined according to the most unfavourable locations obtained from finite element analysis, with consideration of the installation space of equipment. The measuring points of vehicle body acceleration are arranged at the seat bottoms of the middle compartment and the rear car. Equipment such as linear variable differential transform and vibration pickups were used to capture the dynamic signals. General configurations of the on-site test are shown in Figure 4.

Figure 4. Layout diagram of the measuring points. For the car body, vehicle accelerations (Acc.) were tested; for the track beam, vertical displacement (Dis.), vertical and lateral Acc. were tested.

2.2.2 Validation

Before further simulation analysis, the vertical displacement, lateral and vertical acceleration, and lateral and vertical acceleration parameters of the car body were predefined in SIMPACK so that the corresponding postprocessing results could be directly viewed during simulation. The analysis results of the co-simulation model are obtained by observing the dynamic response at the corresponding positions, such as the acceleration and deflection of the lateral vibration of the track beam, as shown in Figure 5.

 doi:10.20944/preprints202409.0428.v1

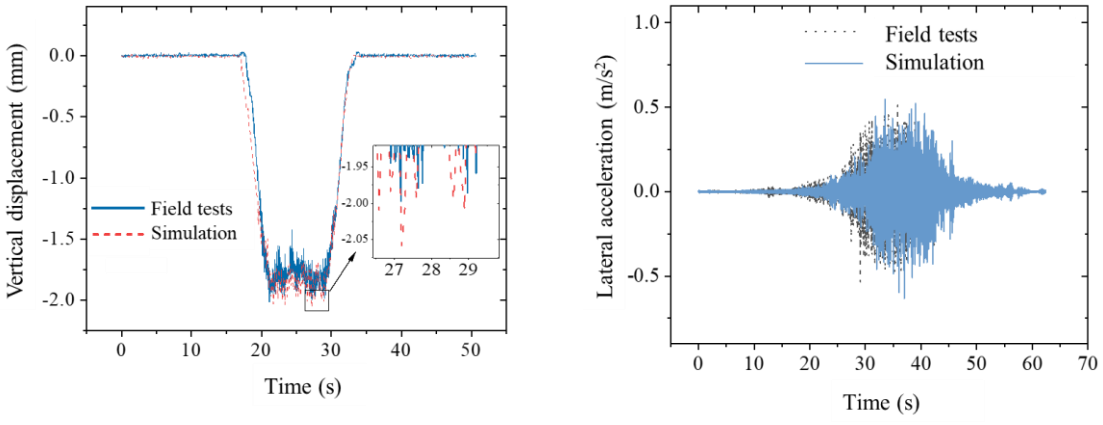

(a) (b)

Figure 5. Comparison of tested and simulation results at the mid-span of a track beam. (a) Vertical displacement; (b) Lateral acceleration.

Analysis of Figure 5 reveals that the simulation results and test results are in good agreement. The simulated vertical displacement of the monorail beam midspan was slightly larger than the actual measured value, which was mainly because the model did not consider the influence of some stiffeners. The analysis results prove that the co-simulation model constructed in this study via ABAQUS and SIMPACK has high accuracy and can be applied to subsequent analysis.

3. Results and Analysis

3.1. Influencing Factors

In the dynamic analysis of vehicle–bridge coupling, with reference to relevant codes, various indexes that representing the dynamic response of MTTS were selected. The evaluation indexes of the dynamic response of track beams are: i) horizontal and vertical deflection at the beam mid-span; ii) acceleration at the beam mid-span; and iii) lateral displacement at the pier top. The evaluation indexes of the dynamic response of monorail trains are: i) wheel unloading rate; ii) acceleration of car body; iii) riding quality); and iv) index of tire stress. It should be noted that the last index is only applicable in monorail systems that utilizing rubber tires.

Main factors influencing the dynamic response of MTTS are the speed of the tourist vehicles, vehicle loadings, the pier height and lateral stiffness of monorail bridge. To lay a solid basis to subsequent analyses, effects of these four influencing factors are firstly analysed in the following.

3.1.1. Effects of Travelling Speed

At present, the MTTS generally serves as an amusement facility, and the maximum speed is 40 km/h under current specifications. In this work, the maximum speed used was km/h, about 1.2 times the maximum operating speed. A total of 10 intervals of vehicle speed were set: 5, 10, …, 50 km/h, so that a comprehensive analysis on the dynamic response can be performed. The model described in Section 2 is then used, with consideration of train loading (maximum capacity), wind loading, and track irregularities. Dynamic responses of the track beam and monorail train are shown in Figure 6.

Preprints.org (www.preprints.org) | NOT PEER-REVIEWED | Posted: 5 September 2024 doi:10.20944/preprints202409.0428.v1

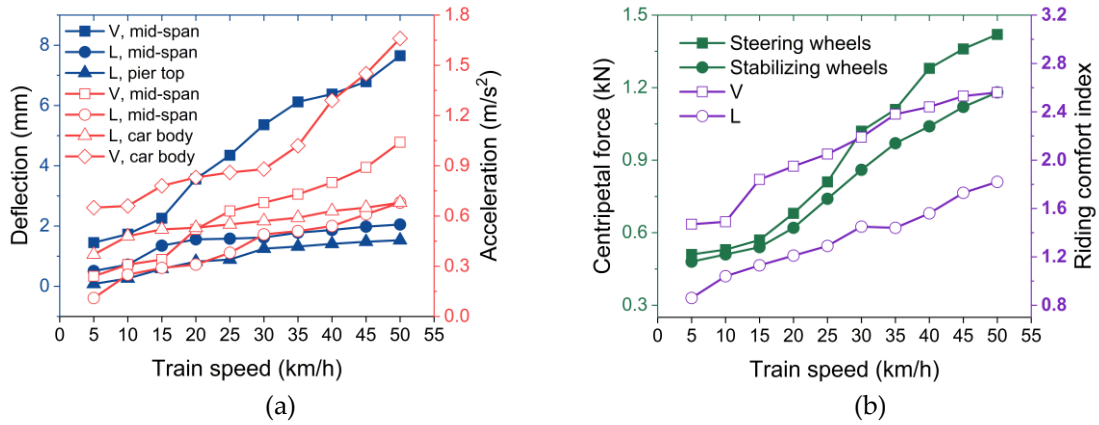

Figure 6. Response results corresponding to different vehicle speeds. (a) Displacement and acceleration response (b) centripetal force and the calculated riding comfort index. Note V and L denote vertical and lateral, respectively.

Figure 6 shows that each kind of dynamic responses continuously increases with vehicle speed. Compared with the other responses, vertical deflection at the mid-span and the vertical acceleration of car body varied significantly with the train speed, indicating that the train speed had the most significant effects on the two. In addition, a significant change of various dynamic responses can be found under a train speed from 20 to 30 km/h. Moreover, in terms deflection and acceleration, vertical responses are more sensitive to the variation of train speed compared to lateral responses, which is also reflected in the curves of riding comfort index in Figure 6b. It should be noted that the steering wheels and stabilizing wheels are located at the webs of the track beam during monorail operation. Hence, similar patterns of centripetal force can be observed.

3.1.2 Effects of Vehicle Loading

To study the effect of vehicle loadings on the dynamic response of MTTS, three different working conditions were used: 1, no load; 2, full load (3.8 tons); and 3, overloaded (5.3 tons). The train speed commonly used in MTTS are divided into three gears: slow, 10 km/h; medium, 20 km/h; and fast, 30 km/h. The rest of the conditions are the same as those described in Section 3.1.1. The dynamic responses of the monorail beam and the vehicle are shown in Figure 7.

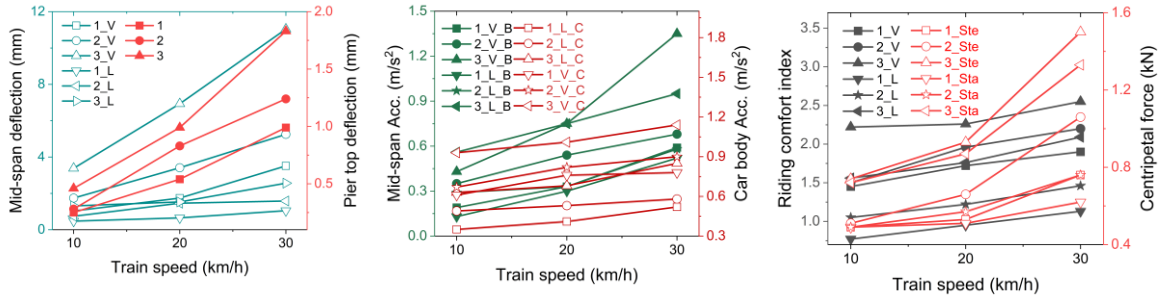

Figure 7. Results under various loading conditions and train speed: (a) Deflection of bridge components; (b) accelerations (c); centripetal force and the calculated riding comfort index. Note 1, 2, and 3 denote the loading conditions; B and C denote bridge and car body, respectively; and Ste and Sta denote steering and stabilizing wheels, respectively.

Figure 7 shows that various types of dynamic response increase as the vehicle loads continuously increases, which are consistent to practical experiences. Specifically, the weight of the vehicle significantly affects the lateral displacement of the pier top, with a greater impact on the vertical deflection at the mid-span than in the lateral direction. Furthermore, this weight has a more

 doi:10.20944/preprints202409.0428.v1

pronounced effect on the vertical acceleration response and vertical stability index compared to the lateral direction.

3.1.3 Effect of Pier Height

In this section, six pier heights of monorail bridge, i.e., 2 m, 4 m, 6 m, 8 m, 10 m and 15 m, were used to analyse the dynamic response of MTTS. The designed maximum train speed (40 km/h) was used in simulations. The rest of the conditions are the same as those described in Section 3.1.1. The dynamic responses of the monorail beam and vehicles are shown in Figure 8.

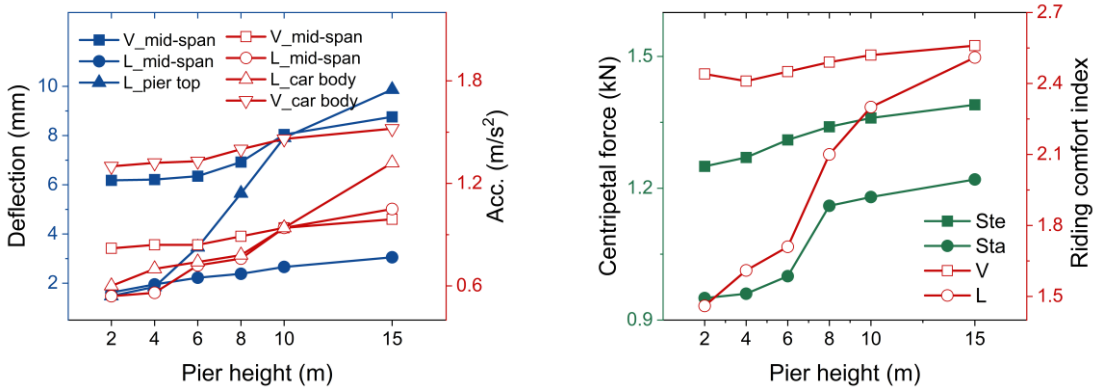

Figure 8. Results under various pier height: (a) Displacement and acceleration response (b) centripetal force and the calculated riding comfort index.

As shown in Figure 8, similar patterns can be found in various dynamic responses versus pier height curves, indicating that the induced dynamic responses generally increase with the increasing pier height. The effect of the pier height on the variation in the lateral displacement of the pier top was more significant than that of the other responses. The variation in the lateral riding comfort index is also significant. Nevertheless, the overall lateral comfort index is less than that of vertical.

3.1.4 Effects of Beam Stiffness

By changing the width and stiffness of the monorail beam, the lateral stiffness of the monorail beam can be altered and hence, effects of lateral stiffness on the track beam can be further investigated. To this end, this work adopted the method of changing the transverse moment of inertia of track beams. The specific method is as follows: the lateral stiffness of the beam *EI* was multiplied by a reduction factor *Rh*, where *Rh* were set to values of 0.3, 0.5, 0.7, 1.0, 1.2, 1.5 and 1.8, to ensure representativeness and coverage of the lateral stiffness of practical track beams. The remaining conditions are as described in 3.1.1. Results are shown in Figure 9.

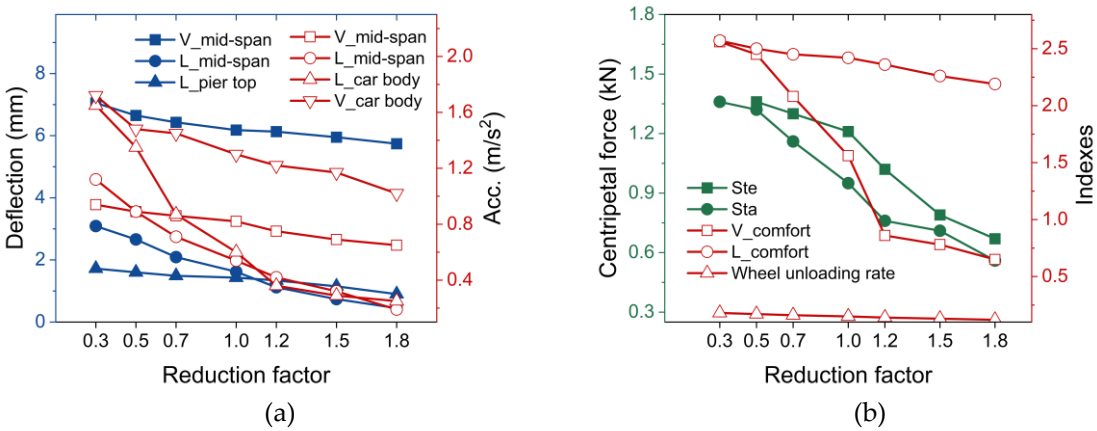

Preprints.org (www.preprints.org) | NOT PEER-REVIEWED | Posted: 5 September 2024 doi:10.20944/preprints202409.0428.v1

Figure 9. Response results corresponding to different reduction factor. (a) Displacement and acceleration responses (b) centripetal force, riding comfort index, and wheel unloading rate.

As shown in Figure 9, all kinds of dynamic response decrease with increasing beam lateral stiffness. The variations in the mid-span lateral deflection and the vehicle body lateral acceleration with the girder lateral stiffness were more significant than the other responses were, and the two kinds of wheel vertical forces and stationarity indicators also varied significantly with the girder lateral stiffness.

3.2 Sensitivity Analysis

3.2.1 Variance-Based Methods

In the variance-based sensitivity analysis, the ratio of the parameter influencing factors to the output variance was calculated to assess the sensitivity of the parameter to the output. In this work, the Sobol index analysis method combined with the Santelli method [29] was used to perform sensitivity analysis. This method uses quasi-random number sequences to construct two random number matrices A and B, then constructs matrix C_i on the basis of A and B, and inputs the parameters of matrices A and B and each row of C_i into the model calculation to obtain three matrices. output vectors u_A, u_B, *and* u_C, from which the first-order sensitivity coefficient S_i and the overall sensitivity coefficient S_{Ti} of the i-th parameter can be calculated. The method is expressed as follows:

$$S_i = \frac{\frac{1}{N}\sum_{j=1}^{N} u_B(j)\left(u_{C_i}(j) - u_A(j)\right)}{E((u_A)^2) - \left(E(u_A)\right)^2} \tag{1}$$

$$S_{T_i} = \frac{\frac{1}{2N}\sum_{j=1}^{N}\left(u_A(j) - u_{C_i}(j)\right)^2}{E((u_A)^2) - \left(E(u_A)\right)^2} \tag{2}$$

3.2.2 Sensitivity Analysis of the Lateral Response

In the sensitivity analysis of the horizontal response, the four influencing factors mentioned above were set as sensitivity input parameters. A MATLAB program was compiled based on the Saltelli method. The sensitivity indicators of each parameter are obtained after the determined parameters are input, as shown in Figure 10.

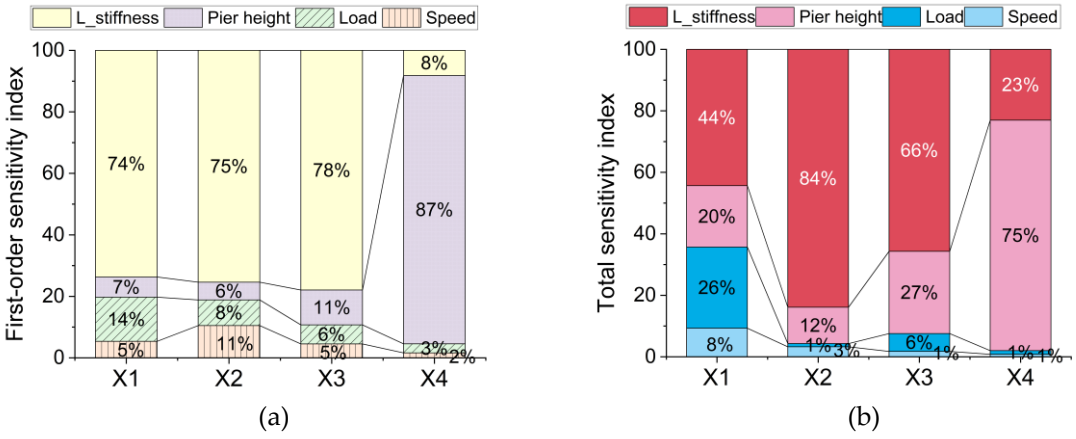

Figure 10. Results of sensitivity indexes: (a) First-order level (b) Total level. Note, X1 represents the vehicle lateral acceleration, X2 represents the lateral displacement at the mid-span, X3 represents the lateral acceleration at the mid-span, and X4 represents the lateral displacement at the pier top.

Preprints.org (www.preprints.org) | NOT PEER-REVIEWED | Posted: 5 September 2024 doi:10.20944/preprints202409.0428.v1

As shown in Figure 10, the height of the monorail girder pier and the lateral stiffness of the beam have the greatest impacts on the lateral response of the overall structure. Among them, the pier height significantly contributes to the lateral displacement of the pier top, accounting for 87% of the first-order sensitivity index and 75% of the total sensitivity index: beam lateral stiffness to car body lateral acceleration and monorail beam midspan. The maximum lateral acceleration and the maximum lateral displacement at the midspan significantly contribute to 74%, 75% and 78% of the first-order sensitivity indicators and account for 44%, 84% and 66% of the total sensitivity indicators, respectively.

3.3 Determination of Lateral Stiffness Index

For the evaluation index of bridge lateral stiffness, the width–span ratio, lateral deflection–span ratio, natural frequency and amplitude are usually chosen. Compared with other indicators, the lateral deflection-to-span ratio can fully reflect the interaction between the vehicle and the bridge system and thus is a more comprehensive indicator for evaluating the performance of bridge structures. Accordingly, the lateral deflection–span ratio is used in the present study to evaluate the lateral stiffness of bridges.

As an important structure in travel and transportation systems, the lateral stiffness limit of the pier column was chosen in the present study as the evaluation scale for the lateral displacement of the pier top. In addition, the mid-span lateral acceleration, stationarity index and wheel lateral force limit are more deterministic; therefore, the above three evaluation criteria are used in the lateral stiffness index in this paper. With reference to other specifications and consideration of structural configurations of MTTS, the evaluation limit of the mid-span lateral acceleration is 0.98 m/s^2; the stability index uses the excellent level limit of the bus stability rating criteria after considering the comfort; and the vertical force limit of the guide wheels is used as the vertical force limit. The evaluation limit was set to 1.37 kN according to the technical conditions of the polyurethane wheel 200–68 tire provided by the manufacturer.

3.3.1 Lateral Acceleration Perspective

Based on the previously obtained data, the maximum transverse acceleration in the span and the transverse displacement at the top of the pier under the variation of the pier height, as well as it's fit to the transverse deflection in the span under the variation of the transverse stiffness are shown in Figure 11.

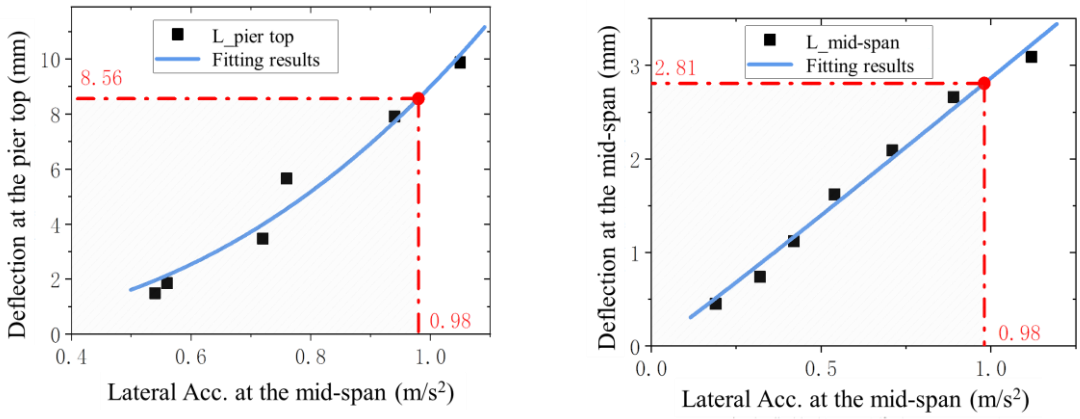

(a) (b)

Figure 11. Fitting results of lateral deflection versus lateral acceleration: (a) Deflection at the pier top (b) deflection at the mid-span.

As shown in Figure 11, the fitting coefficients R^2 of the lateral deflection at the pier top and the mid-span are 0.96 and 0.98, respectively, indicating that the calculated function fits well and can reflect the actual variation patterns of the parameters. Point interpolation was then performed on the

Preprints.org (www.preprints.org) | NOT PEER-REVIEWED | Posted: 5 September 2024 doi:10.20944/preprints202409.0428.v1

basis of the fitting function. When the lateral acceleration at the mid-span was 0.98 m/s2, the lateral horizontal displacement of the pier top was 8.56 mm, and the lateral deflection at the mid-span was 2.81 mm. On the basis of the calculation formula for the lateral deflection–span ratio, the limit of the lateral deflection–span ratio is approximately L/3600.

3.3.2 Lateral Riding Comfort Perspective

Based on the previously obtained results, the fitting results of the lateral stability and the lateral displacement of the pier top under the changes in pier height and lateral deflection under the changes in lateral stiffness are shown in Figure 12.

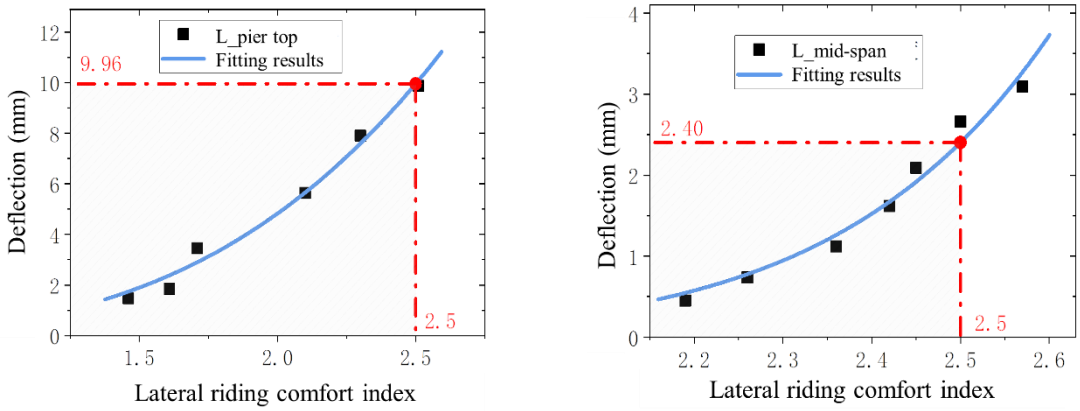

(a) (b)

Figure 12. Fitting results of lateral riding comfort index: (a) lateral displacement at the pier top (b) lateral displacement at the mid-span.

3.3.3 Lateral Wheel Force Perspective

From the data obtained in the previous section, respectively, the vertical force of the guide wheel and the transverse displacement of the top of the pier under the variation of the pier height and it's fit to the transverse deflection under the variation of the transverse stiffness are shown in Figure 13.

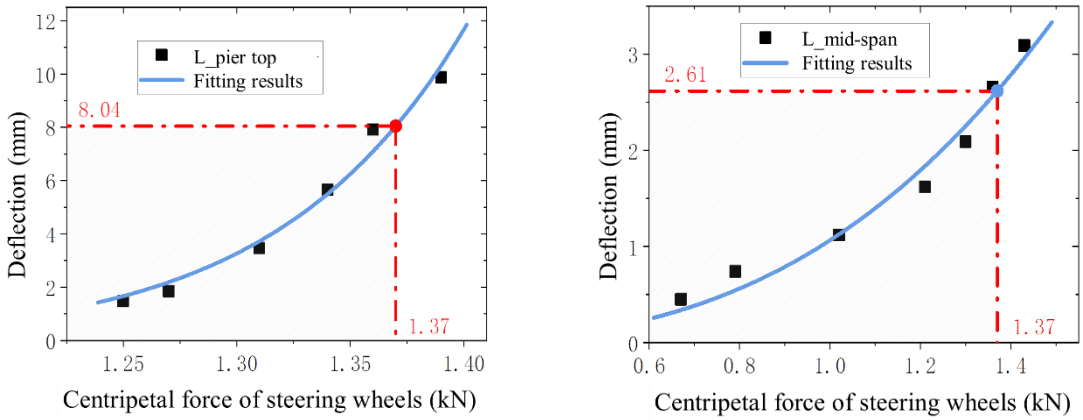

(a) (b)

Figure 13. Fitting results of wheel centripetal force: (a) lateral displacement at the pier top (b) lateral displacement at the mid-span.

The fitting coefficient R^2 of Figure 13a is 0.98, and the fitting coefficient R^2 of Figure 13b is 0.96. According to the fitting function of the selected point interpolation, when the vertical force of the guiding wheel is the limit value of 1.37 kN, the transverse horizontal displacement of the top of the pier takes the value of 8.04 mm, and the transverse deflection in the span takes the value of 2.61 mm.

 doi:10.20944/preprints202409.0428.v1

According to the formula of the transverse lateral deflection-span ratio calculation, it can be obtained that the limit of the lateral deflection-span ratio is about L/3900.

3.3.4 Limits of the Lateral Displacement and Lateral Deflection–Span Ratio of the Pier Top

In the foregoing text, the interpolation method was used to select the values of the fitting function, and the corresponding data are summarized in Table 2.

Table 2. Summary of the lateral deflection and deflection-span ratio limits at the pier top.

Judging criteria	Lateral Acc.	Lateral riding comfort	Wheel lateral force limit
Lateral deflection at the pier top (mm)	8.56	9.96	8.04
Lateral deflection-span ratio	L/3600	L/4200	L/3900

On the basis of the data in Table 2 and considering partial safety, the minimum value of 8.04 mm is used for the lateral displacement of the pier top, and the minimum value of *L*/4200 is taken as the lateral stiffness limit for the lateral deflection–span ratio limit.

4. Discussion

To investigate the difference between the lateral stiffness limit of the MTTS and other specifications, this paper compares the provisions in similar specifications in Table 3. An analysis of the data in Table 3 shows that, among the lateral stiffness limits proposed in this paper, the lateral deflection–span ratio is close to the "Code for the Design of Urban Rail Transit Bridges (GB/T 51234-2017) [4] " and lower than the code of "Design Standards for Straddle-Type Monorail Transit (GB 50458-2022) [3]"; the lateral displacement of the pier top was much lower than those of the other two specifications, which reflects the structural characteristics of the MTTS, which are different from those of rail transportation; therefore, special attention should be given to the design.

Table 3. Comparison of the lateral stiffness limits with specifications (non-mandatory for MTTS)

Specifications	GB 50458-2022	GB/T 51234-2017	MTTS
Lateral deflection at the pier top (mm)	30	25	8.04
Lateral deflection-span ratio	*L*/800	*L*/4000	*L*/4200

5. Conclusions

The main conclusions of this paper are as follows:

(i) A wind-train-bridge coupling model validated by field measurements was developed to investigate the effects of multiple factors on the dynamic response of MTTS. During the changes in vehicle speed and vehicle weight, the vertical response increase of MTTS is greater than the horizontal response increase. Changes in pier height have a significant impact on the lateral response of monorail beams. Moreover, it is concluded that the variation of lateral stiffness can distinctly affect the dynamic responses.

(ii) A variance-based sensitivity analysis was performed on various influencing factors. Results revealed that the pier height and the lateral stiffness significantly affected the lateral response of the overall structure. Among them, the pier height significantly contributed to the lateral displacement of the pier top, accounting for 87% of the first-order sensitivity index and 75% of the total sensitivity index. The lateral acceleration and the maximum lateral displacement at the mid-span significantly contributed to 74%, 75% and 78% of the first-order sensitivity indexes and accounted for 44%, 84% and 66% of the total sensitivity indexes, respectively.

(iii) Based on the obtained results, the lateral responses of MTTS were evaluated in terms of index of beam acceleration, riding comfort of monorail train, and wheel force on the bogie. Finally, two lateral limited values, i.e., lateral displacement limit of 8.04mm for the pier top and the lateral deflection-span ratio limit of L/4200 were determined.

 doi:10.20944/preprints202409.0428.v1

Author Contributions: Methodology, H.Z., P.W., and S.W.; software and formal analysis, P.W. and S.W; data curation, P.W., J.J., and S.W.; writing—original draft preparation, H.Z. and S.W.; writing—review and editing, P.W. and F.G.; supervision and project administration, F.G.; engineering application, Q.L., J.J., C.F., and Q.D. All authors have read and agreed to the published version of the manuscript.

Funding: This research was funded by the National Key Research and Development Program during the 14th Five-Year Plan period of China, grant number 2022YFC3004304.

Data Availability Statement: The data presented in this study may be available on reasonable request.

Conflicts of Interest: Authors Qin Li, Cheng Feng, and Qun Deng were employed by the 3rd Construction Co. Ltd. of China Construction 5th Engineering Bureau. Author Junhui Jin was employed by Zhuzhou CRRC Special Equipment Technology Corporation Limited. The remaining authors declare that the research was conducted in the absence of any commercial or financial relationships that could be construed as potential conflicts of interest.

References

1. Guo, F., Chen, K., Gu, F., et al. The current situation and development of cross seat monorail tourism transportation system in China. *Journal of Central South University (Natural Science Edition)*, **2021**, 52(12): 4540-4551
2. GB 8408-2018; Large-Scale Amusement Device Safety Code. State Administration of Work Supervision: Beijing, China, 2018.
3. GB 50458-2022; Standard for Design of Straddle Monorail Transit. Ministry of Housing and Urban-Rural Development of the People's Republic of China: Beijing, China, 2022
4. GB/T 51234-2017; Code for design of urban rail transit bridge. Ministry of Housing and Urban-Rural Development of the People's Republic of China: Beijing, China, 2017
5. Gao, Q., Cui, K., Li, Z., et al. Numerical investigation of the dynamic performance and riding comfort of a straddle-type monorail subjected to moving trains[J]. Applied Sciences, 2020, 10(15): 5258.
6. Liu, M. Study on Coupling Vibration of Windmill Bridge for T-beam Continuous Rigid Frame Bridge in High Altitude Area. Master's Thesis, Chongqing Jiaotong University, Chongqing, 2019.
7. Miao, Y. Studies on Coupled Vibration of Rail-cum-Road Cable-stayed Bridge with a Super Span under Wind Loads. Master's Thesis, Central South University, Changsha, 2014.
8. Huang, G., Ren, N., Zheng, H. Structural dynamics of bridges under the coupling effect of windmills and bridges. European Journal of Computational Mechanics, 2023, 31(5-6): 601-620.
9. CEHN, J., LI, R., XU, J., et al. Study on the aerodynamic performances and the operational safety of the vehicle-bridge system under the crosswind. Mechanics Based Design of Structures and Machines, 2024, 2: 1-23.
10. WANG, S., WAN, X., GUO, M., et al. Nonlinear dynamic analysis of the wind–train–bridge system of a long-span railway suspension truss bridge. Buildings, 2023, 13(2): 277.
11. ZOU, Y., LIU, Z., SHI, K., et al. Analysis of effects of aerodynamic interference on dynamic response of suspended monorail wind–vehicle–bridge system using joint simulation approach. Structures, 2022, 45: 179-198.
12. LUO, S. The Research on the Aerodynamic Characteristics of Road Vehicles on Bridge Deck and Its Driving Safety. Master's Thesis, Hunan University of Science and Technology, Xiangtan, 2023.
13. JIANG, Y. Study on Coupled Vibration and Lateral Stiffness of Steel Girder Cable-stayed Long-span Road-rail Bridge. Master's Thesis, Chongqing: Chongqing Jiaotong University, 2023.
14. GUO, X., Zou, X. Influence of wind guide railing parameters on wind-vehicle-bridge coupling vibration of steel truss bridge. Journal of Railway Science and Engineering, 2024, 21(03): 1068-1078.
15. Sugimura, H., Takeda, M., Takei, M., Yamaoka, H., & Ogata, T. Development of HEV engine start-shock prediction technique combining motor generator system control and multi-body dynamics (MBD) models. SAE International Journal of Passenger Cars-Mechanical Systems, 2013, 6(2013-01-2007), 1363-1370.
16. XIANG, H., TAO, Y., CHEN, X., et al. Study on Transverse Deflection-span Ratio Limit of Long-span Railway Suspension Bridge Considering Wind Barrier. Journal of the China Railway Society, 2023, 45(03): 62-69.
17. ZHOU, C., XU, X., ZHENG, X., et al. Study on the Influence of Pier Stiffness on Vehicle-bridge Coupled Vibration of Long-span Continuous Girder Bridge of Railway. High Speed Railway Technology, 2022, 13(06): 23-29.
18. ZHU, Z., JIANG, Z. Analysis of dynamic characteristics of large-span suspension bridges with extended spans of stiffening girders. Journal of Railway Science and Engineering, 2022, 19(04): 1014-1023.
19. LIU, L., JIANG, L., LIU, X., et al. Research on analytical model of transverse deformation and rail surface deformation of high-speed railway bridge based on Ritz method. Journal of Central South University (Natural Science Edition), 2021, 52(12): 4349-4360.

 doi:10.20944/preprints202409.0428.v1

20. WANG, M., SONG, Z., TENG, N. Research on Transverse Stiffness of High Speed Maglev Guideway Girder Based on Coupled Vibration. Railway Engineering, 2021, 61(08): 1-5.
21. YAN, Y., ZHAN, J., ZHANG, N., et al. Influence of Pier Transverse Displacement and Foundation Stiffness Change on High Speed Running Safety. Railway Engineering, 2020, 60(10): 8-12.
22. CARDEN, L.P., BUCKLE, I.G., ITANI, A.M. Transverse displacement capacity and stiffness of steel plate girder bridge superstructures for seismic loads. Journal of Constructional Steel Research, 2007, 63(11): 1546-1559.
23. Naeimi, M., Tatari, M., Esmaeilzadeh, A., & Mehrali, M. Dynamic interaction of the monorail–bridge system using a combined finite element multibody-based model. Proceedings of the Institution of Mechanical Engineers, Part K: Journal of Multi-body Dynamics, **2015**, 229(2), 132-151.
24. Guo, F., & Wang, P. Measurement and analysis of the longitudinal level irregularity of the track beam in monorail tour-transit systems. Scientific Reports, **2022**, 12(1), 19219.
25. Wang, P., Guo, F., Zhang, H., Jin, J., Liao, Q., & Yan, Y. Acquiring the High-Precision Spectrum of Track Irregularity by Integrating Inclination in Chord Methods: Mathematics, Simulation, and a Case Study. Mathematics, **2024**, 12(14), 2227-7390.
26. Jiang, Y., Wu, P., Zeng, J., Qu, S., Wang, X., & Wang, S. Simplified and relatively precise back-calculation method for the pavement excitation of the monorail. International Journal of Pavement Engineering, **2021**, 22(4), 480-497.
27. Naeimi, M., Tatari, M., Esmaeilzadeh, A., & Mehrali, M. Dynamic interaction of the monorail–bridge system using a combined finite element multibody-based model. Proceedings of the Institution of Mechanical Engineers, Part K: Journal of Multi-body Dynamics, **2015**, 229(2), 132-151.
28. Shamsi, M., & Ghanbari, A. Nonlinear dynamic analysis of Qom monorail bridge considering soil-pile-bridge-train interaction. Transportation Geotechnics, **2020**, 22, 100309.
29. Saltelli, A., Tarantola, S., and Chan, K. A quantitative model-independent method for global sensitivity analysis of model output. *Technometrics*, **1999**, 41.1: 39-56.